J Mater Sci (2007) 42:9511–9523
DOI 10.1007/s10853-007-1757-9

INTERFACE SCIENCE

Solidification contact angles of molten droplets deposited on solid surfaces

Ri Li · Nasser Ashgriz · Sanjeev Chandra · John R. Andrews

Received: 4 February 2007 / Accepted: 9 April 2007 / Published online: 23 June 2007

Abstract Droplet impact and equilibrium contact angle have been extensively studied. However, solidification contact angle, which is the final contact angle formed by molten droplets impacting on cold surfaces, has never been a study focus. The formation of this type of contact angle was investigated by experimentally studying the deposition of micro-size droplets (~39 μm in diameter) of molten wax ink on cold solid surfaces. Scanning Electron Microscope (SEM) was used to visualize dots formed by droplets impacted under various impact conditions, and parameters varied included droplet initial temperature, substrate temperature, flight distance of droplet, and type of substrate surface. It was found that the solidification contact angle was not single-valued for given droplet and substrate materials and substrate temperature, but was strongly dependent on the impact history of droplet. The angle decreased with increasing substrate and droplet temperatures. Smaller angles were formed on the surface with high wettability, and this wetting effect increased with increasing substrate temperature. Applying oil lubricant to solid surfaces could change solidification contact angle by affecting the local fluid dynamics near the contact line of spreading droplets. Assuming final shape as hemispheres did not give correct data of contact angles, since the final shape of deposited droplets significantly differs from a hemispherical shape.

R. Li · N. Ashgriz (✉) · S. Chandra
Department of Mechanical and Industrial Engineering, University of Toronto, 5 King's College Road, Toronto, Ontario, Canada M5S3G8
e-mail: ashgriz@mie.utoronto.ca

R. Li
e-mail: ril@mie.utoronto.ca

J. R. Andrews
Xerox Corporation, Wilson Center for Research and Technology, 800 Phillips Rd. M/S 114-44D, Webster, NY 14580, USA

Nomenclature

C_p	Specific heat of droplet
D	Diameter of spherical droplet
G	Shear modulus of substrate
h	Height of sessile droplet
H	Elastic displacement of viton surface
k_0	Thermal conductivity of substrate
k_c	Thermal conductivity of substrate coating
k_d	Thermal conductivity of droplet
l	Thickness of substrate coating
L	Flight distance of droplet
L_f	Latent heat of fusion of droplet
R_c	Thermal resistance of substrate coating
R_d	Thermal resistance of droplet
t	Time
t_{solid}	Solidification time scale of droplet
t_{spr}	Spreading time scale of droplet
T_d	Droplet temperature upon impact
T_j	Jetting temperature
T_m	Droplet melting temperature
T_s	Substrate temperature
U	Velocity of droplet upon impact
X	Thickness of solidified layer

Greek symbols

α_0	Thermal diffusivity of substrate
α_d	Thermal diffusivity of droplet
θ_c	Calculated contact angle of sessile droplet
θ_e	Equilibrium contact angle

θ_l Contact angle measured on the left of photographs
θ_r Contact angle measured on the right of photographs
θ_s Solidification contact angle
λ Parameter defined in Eq. 7
μ Viscosity of droplet
ρ Density of droplet
σ Surface tension of droplet

Dimensionless numbers

Ca $\mu\ U/\sigma$ (Capillary number)
Pr $\mu\ C_p/k_d$ (Prandtl number)
Re $\rho\ UD/\mu$ (Reynolds number)
Ste $C_p(T_m–T_s)/L_f$ (Stefan number)
We $\rho\ U^2D/\sigma$ (Weber number)
β $(T_d–T_m)/(T_m–T_s)$ (Superheat parameter)

Introduction

Deposition of small molten droplets on cold solid surfaces is the central research topic in many industrial applications, which include thermal spray coating [1, 2], soldering [3–5], micro-fabrication [6], and solid-ink printing [7]. Solid-ink printing technology, to which the present study is directly relevant, is widely used to print high-quality color images. Wax ink (also called solid ink or phase change ink), typically a wax in which colored dyes are dissolved, is ejected in the form of small droplets (~20–40 μm diameter) from a heated piezoelectric printhead onto a rotating metal drum. The droplets land on the drum in a pattern that makes up the image and solidify to form hemispherical bumps (or ink dots) (see Fig. 1a). The drum is then rolled over a sheet of paper to which the ink droplets cling, transferring the entire image onto the paper. Figure 1b shows flattened ink dots sticking to photo paper.

The quality of images formed depends on the shape of the ink dots deposited on the drum. One of the important shape parameters of the ink dots is the contact angle, which can affect the process of flattening (or transfixing) ink dots onto the paper. In an isothermal droplet impact problem where the droplet and substrate have the same temperature, the droplet finally reaches a thermodynamic equilibrium state, which can be characterized by an equilibrium contact angle (θ_e). This parameter is determined by droplet material, substrate material, and temperature. However, in the case of molten droplets impacting on cold surfaces such as the present work, equilibrium contact angles do not exist due to the non-existence of three-phase lines. The final contact angle formed under such thermally non-equilibrium conditions is referred to as solidification contact angle (θ_s), which has been the focus of the present work. The

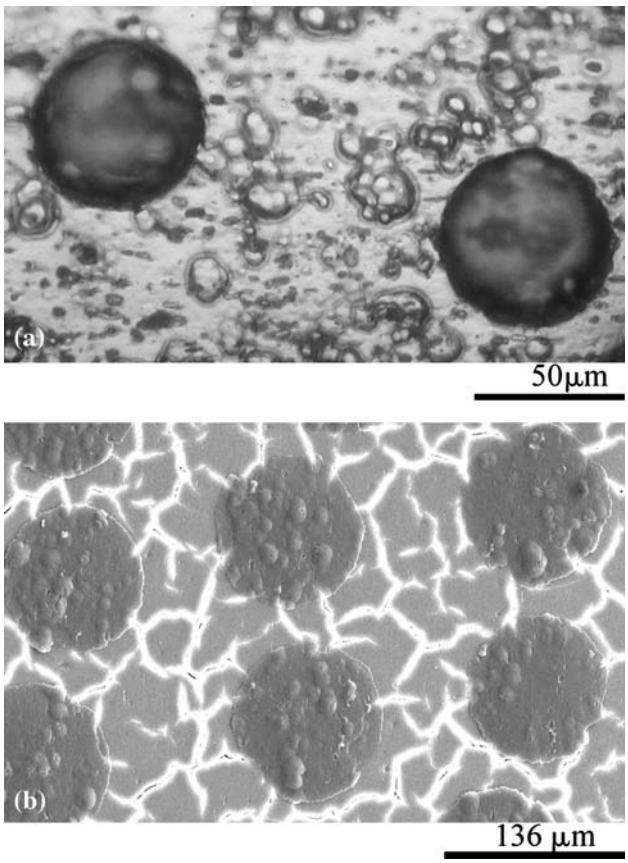

Fig. 1 (**a**) Optical microscopic images of ink dots formed by droplets of hot-melt ink deposited on an intermediate drum (Smaller dots on the figure are cavities on the drum surface); (**b**) the dots were flattened on photo paper when transferred from the drum

formation of θ_s is a result of complex process in which heat transfer, solidification and deformation of droplet occur simultaneously. Hence, θ_s will be sensitive to all the impact conditions, reflecting the thermal and flow histories of droplets during impact.

The impact of droplet on solid surfaces has been extensively studied, and many of early works [8–13] focused on the evolution of spreading diameter and splat height. Much attention has been paid to the apparent dynamic contact angle in the case of isothermal impact [14–16], while little work has been done on the apparent contact angle when solidification is involved.

Gao and Sonin [6] modified an ink-jet printer to shoot wax droplets on a flat target and introduced the concept of solidification contact angle. It was noted that, as long as spreading was completed much faster than solidification, the solidification contact angle depended mainly on droplet and substrate materials and substrate temperature, and was independent of spreading history. Schiaffino and Sonin [17] studied apparent dynamic contact angles formed by continuous deposition of droplets on a homologous

substrate. In the case of negligible effect of inertia and domination of capillary and viscous forces, it was found that the apparent dynamic contact angle seems to obey Hoffman's law [18]. Attinger et al. [3] recorded the evolution of dynamic contact angle during the deposition of molten solder droplets on solid substrates, and concluded that the contact angle dynamics was strongly coupled to the evolution of the droplet free surface and no quantitative agreement with Hoffman's law. Schiaffino and Sonin [19] observed that the post-solidification shape of mercury droplets deposited on frozen mercury changed with Stefan number (Ste) and superheat parameter (β), without separating the effects of the two parameters. The two dimensionless parameters are expressed by

$$\mathrm{Ste} = \frac{C_p(T_\mathrm{m} - T_\mathrm{s})}{L_\mathrm{f}} \tag{1}$$

$$\beta = \frac{T_\mathrm{d} - T_\mathrm{m}}{T_\mathrm{m} - T_\mathrm{s}} \tag{2}$$

where C_p, L_f, and T_m are specific heat, latent heat of fusion and melting temperature of droplet, T_d and T_s are pre-impact temperatures of droplet and substrate. The analytical model in [19] for solidification contact angle of droplets (homologous, $\mathrm{We} = \rho U^2 D/\sigma \ll 1$, negligible viscosity effect) considered only the material and Stefan number. Bhola and Chandra [20] observed the apparent dynamic contact angle of single molten paraffin wax droplets (~2 mm diameter) impacting on an aluminum surface with three substrate temperatures (T_s). With T_m = 70 °C, impaction under T_s = 40 and 73 °C ended up with the same contact angles (θ_s) equal to the equilibrium contact angle (θ_e) at 73 °C, while a larger contact angle was formed under T_s = 23 °C.

Although some early works have reported some sparse information on solidification contact angle, there is still no systematic study on this topic. This work considered single droplets of hot-melt ink impacted on solid surfaces, and investigated the effects of substrate temperature, flight distance of droplets (the distance between droplet generator and substrate) and initial temperature on θ_s. Different types of substrates were used in our tests to examine the effect of non-stick coating and lubricant that are usually applied to drum surface in solid-ink printers to ensure easy detachment of ink droplets.

Experimental method

A Phaser 860 printhead (Xerox Corporation, Rochester, NY) was modified as a droplet generator to eject droplets horizontally towards a substrate, which was a polished aluminum plate (50 mm × 5 mm × 5 mm in size) mounted on a moving stage. After each droplet was deposited, the stage was moved by 150 μm so as to deposit the next droplet on a clean portion of the surface. Both droplet generator and substrate were heated with cartridge heaters inserted into them and their temperatures regulated with an accuracy of ±0.5 °C using temperature controllers. Substrate temperature (T_s) was varied from 60 to 80 °C in increments of 5 °C. The temperature of droplet generator, which is the temperature of droplet at the instant of generation and referred to as jetting temperature (T_j), was maintained at either 140 or 145 °C.

Figure 2a shows a droplet, initially at temperature T_j, being ejected towards the substrate at temperature T_s. The distance between the droplet generator and substrate surface, referred to as flight distance of droplet (L), was kept at either 0.5 or 1.0 mm. Three types of substrates were used. The first was a bare aluminum plate with average roughness 0.05 μm, which is referred to as the uncoated substrate hereinafter. The second was coated with 1.8 μm thick layer of Viton (DuPont Corporation, Wilmington, DE), the proprietary name of a fluoroelastomer that is heat resistant to 200 °C and is applied to drums in printers to reduce adhesion of wax droplets. The Viton coating did not measurably change surface roughness. This substrate is called viton-coated substrate hereinafter. The third was an oil-coated substrate, which was prepared by wiping a bare aluminum surface with a cloth soaked in silicone oil, leaving an oil layer approximately 1 μm thick on the surface. All experimental conditions are listed in Table 1. Each case was conducted for five different substrate temperatures (T_s).

ColorStix 8200 manufactured by Xerox Corporation (Rochester, NY), a typical commercially used wax ink, was used as droplet material. The material melts over a temperature range of 60–115 °C. However, its viscosity (μ) changes over a narrow temperature range. Figure 2b shows that the viscosity of ColorStix 8200 sharply increases when temperature drops below 90 °C. This temperature can be considered the effective melting point of the ink (T_m). Figure 2b also shows that surface tension of this ink (σ) changes slightly and linearly with temperature above this melting temperature: the surface tension of ColorStix 8200 was measured to be 0.02554 N/m at 140 °C and 0.02645 N/m at 120 °C. Table 2 lists the properties of ColorStix 8200, aluminum, viton, and silicon oil.

After a droplet landed on a substrate surface, it was allowed to stay at the substrate temperature for approximately 5 min, and then allowed to cool to room temperature. Photographs showed that there was no observable change in droplet shape during this cooling period. Solidified droplets were examined using both optical and scanning electron microscopy (SEM). Droplets were

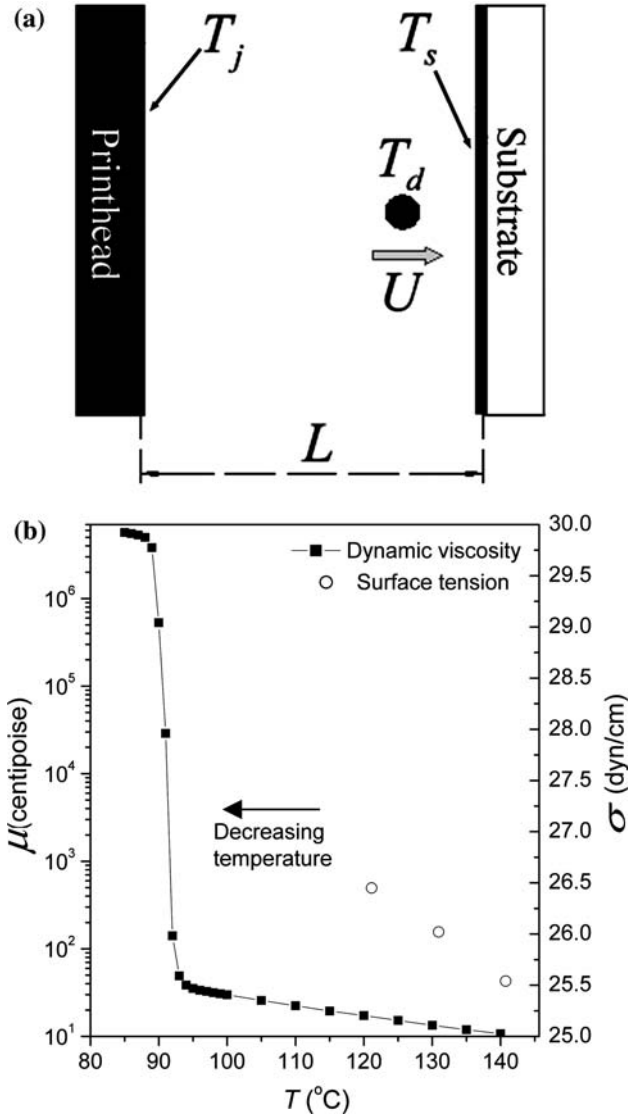

Fig. 2 (**a**) The schematic shows that a droplet is generated by a droplet generator (modified from a printhead), travels a distance L and impacts on a solid surface; (**b**) dynamic viscosity and surface tension of ColorStix 8200 varying with temperature

Table 1 Experimental tests carried out with varied conditions

Tests	Substrate	L (mm)	T_j (°C)
Case I	Uncoated	0.5, 1	140
Case II	Viton-coated	0.5, 1	140
Case III	Oil-coated	0.5	140
Case IV	Uncoated	1	145

sputter-coated with gold before being placed in the SEM; their temperature was kept well below 60 °C during the coating process to avoid any phase change.

A high-speed video camera (FASTCAM-ultima 1024, Photron Ltd.) was used with a microscope lens (QM 100, Questar) to photograph droplets in flight with a frame rate of 16,000 fps (frames per second). Droplet diameter (D) and velocity (U) were measured from these images. Droplets of ColorStix 8200 had an average diameter of 39 ± 0.4 μm, based on measurements of 10 droplets. Droplet velocity was measured by tracking change in droplet position from high speed video images. By averaging measurements from ten droplets, the average velocity at $L = 0.5$ mm was 2.81 ± 0.07 m/s, decreasing to 2.56 ± 0.04 m/s at $L = 1$ mm. Droplets were elongated as they emerged from the orifice of the droplet generator, but became spherical in less than 50 μs due to surface tension, so that they were always spherical at the instant of impact.

Table 2 Properties of droplet and substrate materials

Material	ρ (kg m^{-3})	C_p (kJ kg^{-1} K^{-1})	k (W m^{-1} K^{-1})	L_f (kJ kg^{-1})	T_m (°C)
ColorStix 8200	820	2.25	0.18	183	90
Aluminum	2770	0.875	177	–	–
Viton	1915	955	0.17	–	–
Silicon oil	–	–	0.1	–	–

Air temperature in the gap between the substrate and droplet generator was measured using a 0.3 mm diameter thermocouple probe (HYP-1, Omega Engineering, Stamford, CT) mounted on a micrometer stage. In-flight cooling of droplets due to forced convection was calculated numerically by neglecting temperature gradients in droplets (the Biot number was less than 0.1) and using measured values of droplet velocities and air temperatures. Results showed that the droplet temperature decreased from $T_j = 140$ °C to $T_d = 136$ °C at $L = 0.5$ mm and $T_d = 132$ °C at $L = 1$ mm. These values were assumed to be initial droplet temperatures at impact (T_d).

Drop-shape analysis software (ImageJ with DropSnake and LB-ADSA plug-ins) was used to measure the apparent contact angle by finding the local tangent angle on the droplet edge. The method was illustrated in Fig. 3. The angles on the left (θ_l) and right (θ_r) were measured, the average of which was taken as θ_s.

Experimental results

Contact angle (θ_s) versus substrate temperature (T_s) and flight distance (L)—Case I

A static contact angle formed by a liquid drop sitting on a solid surface is the equilibrium contact angle (θ_e), which depends on temperature for a given liquid and a solid

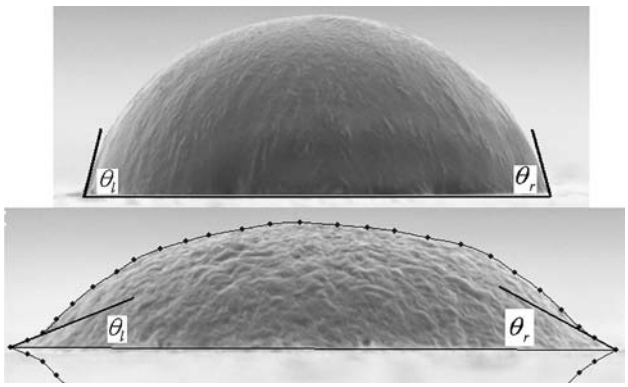

Fig. 3 For each ink dot formed, two apparent contact angles (θ_l, θ_r) were measured, and the average of these two angles was taken as θ_s

material. Figure 4a shows this type of contact angle for molten ColorStix 8200 on the uncoated aluminum surface, which was produced by placing a small piece of ink wax (m = 0.2 mg) on a heated substrate. Since its bond number [$\mathrm{Bo} = (36m^2\rho/\pi^2)^{1/3}g/\sigma = 0.17$] was much less than unity, gravitational effect was negligible. It can be seen that the liquid spreads out like a thin layer with a small contact angle. Liquid spread increased with increasing temperature. In comparison to Fig. 4a, a sharp contrast can be seen in Fig. 4b and c, which shows droplets of ColorStix 8200 impacted on the uncoated substrate with the substrate located at L = 0.5 mm (Fig. 4b) and 1 mm (Fig. 4c) from the droplet generator. Quite obviously, the solidification contact angles formed in Fig. 4b and c are much larger than the equilibrium contact angles in Fig. 4a, indicating the solidification contact angles were formed under non-equilibrium conditions.

The contact angles of ink drop shown in Fig. 4a were measured and plotted versus temperature in Fig. 5a, which

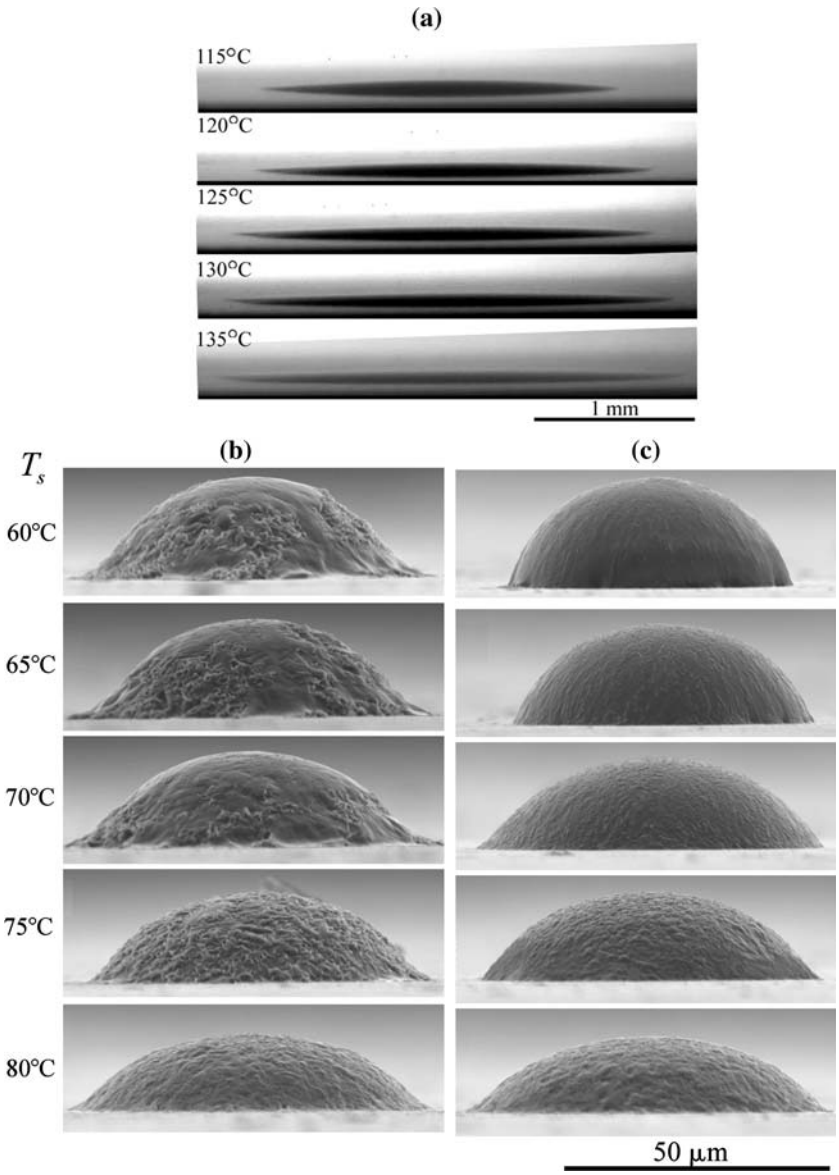

Fig. 4 (**a**) Equilibrium shapes of a molten ink drop (m = 0.2 mg, Bo = 0.17) at varied temperatures; (**b**, **c**) side view SEM images of ink dots formed on the uncoated substrate (T_j = 140 °C, Case I): (**b**) L = 0.5 mm; and (**c**) L = 1 mm

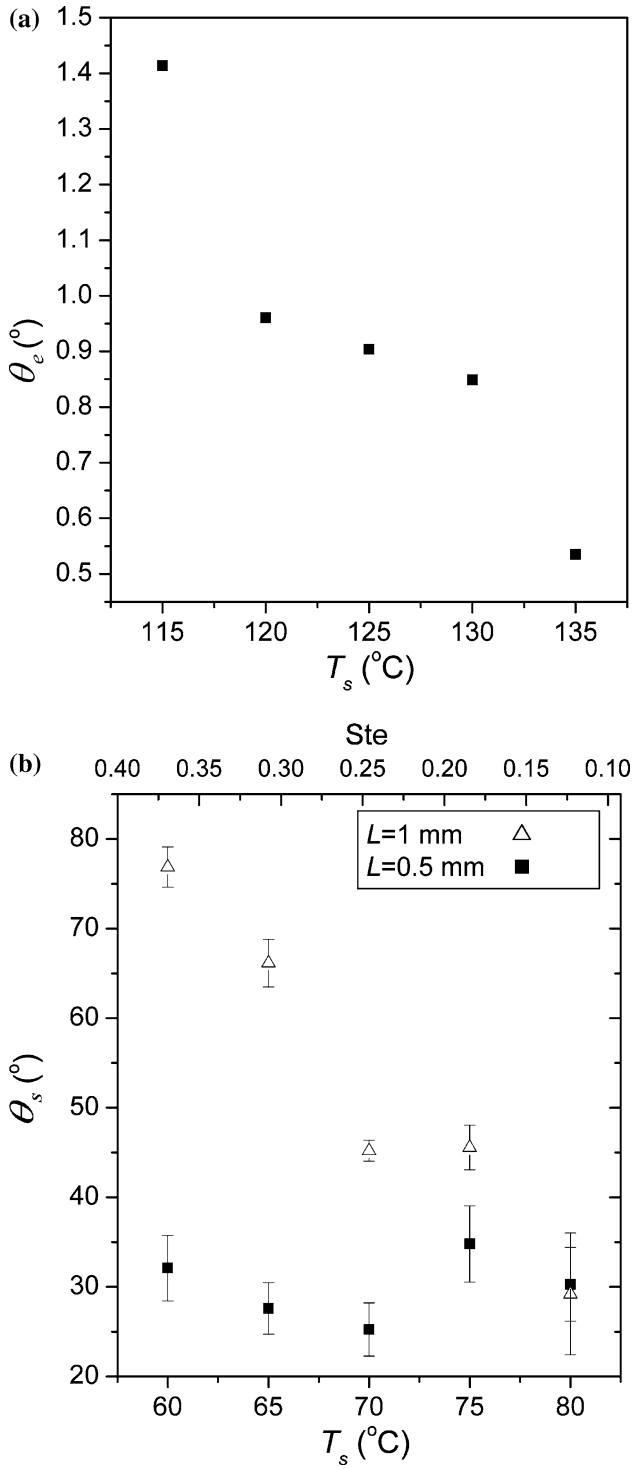

Fig. 5 (**a**) Equilibrium contact angle (θ_e) of ColorStix 8200 on the uncoated aluminum surface at varied temperatures; (**b**) solidification contact angles (θ_s) formed on the uncoated substrate with T_j = 140 °C (Case I) versus substrate temperature and Stefan number [Ste = $C_p(T_m - T_s)/L_f$]

clearly establishes that θ_e decreases with increasing temperature. Through choosing a few pieces of ink with different masses and linearly fitting the measurements to zero Bond number, the equilibrium contact angle of ColorStix 8200 on aluminum surface was found to be around 1 at 120 °C (similar to the method used in [21]). Solidification contact angles in Fig. 4b and c were measured and plotted as a function of T_s and Ste in Fig. 5b. For L = 1 mm, θ_s decreased with increasing T_s (decreasing Ste), while for L = 0.5 mm, θ_s did not change much with T_s. The angles formed at L = 1 mm were larger than those at L = 0.5 mm, and the difference diminished as T_s increased.

Discussion

During the process of impact, droplet is forced to spread out by inertia force, and the spreading is opposed by surface tension and viscous forces. It was concluded that surface tension effect dominates the termination of droplet spreading over viscous effect when [9]

$$\mathrm{We} \ll 2.8\,\mathrm{Re}^{0.457} \tag{3}$$

where Reynolds number is $\mathrm{Re} = \rho UD/\mu$. In the present work, using the properties of the ink at 140 °C, Weber number was around 8, and Reynolds number was around 7. Hence, the right hand side of Eq. 3 is around 7, showing a significant effect of viscous dissipation. It should be noticed that We and Re were calculated based on physical properties at T_j = 140 °C. Viscous effect could be more dominant during the spreading process since μ has a stronger temperature dependency than σ (see Fig. 2).

Since the evolution of contact angle is affected by fluid dynamics and change of physical properties of the liquid adjacent to contact line, it might be more proper to compare the surface tension and viscosity effects near the contact line. This is in fact the form of capillary number (Ca), which under non-isothermal conditions is expressed by

$$\mathrm{Ca}(T) = \frac{\mu(T)u}{\sigma(T)} \tag{4}$$

where viscosity and surface tension are temperature dependent, and u is the instantaneous contact line velocity. Hoffman's law [18] correlated the apparent dynamic contact angle of isothermally spreading droplets with θ_e and Ca. Although Attinger et al. [3] found no quantitative agreement with Hoffman's law in their work of solder droplets impacting on wafer, the qualitative meaning of Hoffman's law still holds for non-isothermal droplet spreading.

For a spreading droplet, the velocity u refers to the velocity of the moving contact line. In the case of isothermal droplet impact, the impaction starts with an inertia-driven process followed by a spontaneous process, which is driven by capillary forces. For droplets impacting on cold

solid surfaces with phase change, solidification starts at the droplet–substrate interface (as will be seen in Fig. 7). The occurrence of solidification makes the spreading process mainly driven by inertia. Therefore, the average speed of contact line during spreading is in the same order of magnitude as U. In view of this, the velocity u was approximated by the droplet impact velocity (U). The variations of μ and σ with temperature as shown in Fig. 2 were used to evaluate the change of capillary number with temperature. Since σ was measured only at three temperature points, linear interpolation and extrapolation were applied to estimate surface tension at other temperature points. The results were presented in Fig. 6 using $U_{L=0.5} = 2.81$ m/s, where one can see that Ca increases linearly from 1.2 at 140 °C to 3.9 at 94 °C and sharply increases afterwards. It is worth mentioning that the highest substrate temperature used was 80 °C. This indicates that surface tension had a minor effect at the beginning of droplet impact, and viscous effect dominated as the process of impact proceeded. Therefore, the droplet impaction was a coupling process of viscous damping and impact inertia.

Figure 5b shows the effect of distance L on θ_s. Since viscous effect is a major factor, the effect of L can be evaluated by considering the pre-impact Reynolds number of droplets

$$\frac{\mathrm{Re}_{L=0.5}}{\mathrm{Re}_{L=1}} = \frac{U_{L=0.5}\mu_{L=1}}{U_{L=1}\mu_{L=0.5}} \tag{5}$$

Interpolating from Fig. 2b, μ is 11.5 cps at $L = 0.5$ mm (T_d = 136 °C) and 12.7 cps at $L = 1$ mm (T_d = 132 °C).

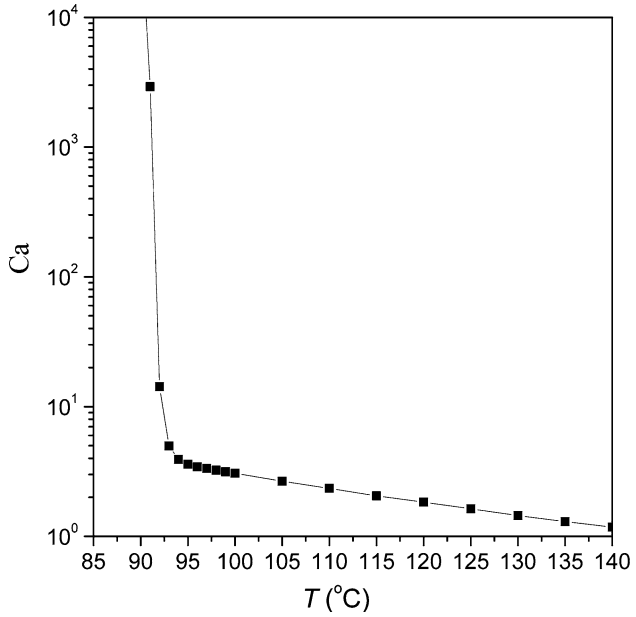

Fig. 6 Variation of capillary number ($\mathrm{Ca} = \mu U/\sigma$) with temperature ($U$ = 2.81 m/s)

The Reynolds number ratio was around 1.22, which indicates that the viscous damping had more effect at L = 1 mm. A detailed discussion on the effect of L will be provided later.

Solidification is another major factor, which has not been considered. To evaluate the effect of solidification, we can start by carrying out a time scale analysis. Droplet spreading is driven by inertial forces, and the time required for spreading of a liquid droplet (t_{spr}) can be estimated by [19]:

$$t_{spr} = \frac{D}{U} \tag{6}$$

For the experimental conditions in this study $t_{spr} \sim 15$ μs. The time required for the whole droplet to solidify can be approximately estimated by considering one-dimensional heat conduction between two semi-infinite bodies [22]. The transient location of solidification front is expressed by

$$X = 2\lambda\sqrt{\alpha_d t} \tag{7}$$

where, α_d is thermal diffusivity of the ink, the parameter λ is a function of superheat parameter (β), Stefan number (Ste), and the thermal properties of ink and substrate. Assuming properties of the ink do not change with phase (solid and liquid), this function is expressed by

$$\left[\frac{\beta}{erfc(\lambda)} + \frac{\lambda e^{\lambda^2}\sqrt{\pi}}{\mathrm{Ste}}\right]\left[\frac{k_d}{k_0}\sqrt{\frac{\alpha_0}{\alpha_d}} + erf(\lambda)\right] = 1 \tag{8}$$

where k_0 and α_0 are thermal conductivity and diffusivity of aluminum, and k_d thermal conductivity of the ink.

Using the droplet diameter (D) as the characteristic length, the bulk solidification time of droplet (t_{solid}) is

$$t_{solid} = \frac{D^2}{4\lambda^2\alpha_d} \tag{9}$$

Hence, the ratio of the two time scales is

$$\frac{t_{spr}}{t_{solid}} = \frac{4\lambda^2}{\mathrm{Re\ Pr}} \tag{10}$$

where Re ~ 7 and Prandtl number $\mathrm{Pr} = \mu C_p/k_d \sim 131$ in our tests, using properties of the ink at 140 °C. Substitution into Eq. 10 gives $3 \times 10^{-4} < t_{spr}/t_{solid} < 4 \times 10^{-5}$, indicating that the droplet would solidify completely long after it had spread to its maximum extent.

Based on the foregoing analysis, it seems that, in the present work, solidification was not a significant factor in affecting the final bulk shape of impacted droplets. However, a solidified layer, which appeared and grew at the droplet–substrate interface, could greatly influence the

evolution of free surface adjacent to the contact line. The thickness of this solidified layer at the point of maximum spread can be estimated by submitting Eq. 6 into Eq. 7, which gives

$$X_{t=t_{spr}} = 2\lambda\sqrt{\frac{\alpha_d D}{U}} \tag{11}$$

Equation 11 is plotted in Fig. 7 as a function of T_s for $L = 0.5$ and 1 mm. The formation and growth of this layer opposed both spreading and receding of contact line, thereby arresting the contact line. The arrest of contact line with the rest of the droplet still in motion could significantly change the evolution of the free surface near the contact line, and the solidification contact angle, therefore, was affected. The presence of solidified layer also changed the contact between droplet and substrate surface, which otherwise would have remained as a liquid–substrate contact.

The discussion above could also be helpful to understand two previous works: Schiaffino and Sonin [17] reported an agreement between Hoffman's law and their results of droplets impacting on the same frozen material; while Attinger et al. [3] found no such an agreement in their work of solder droplets impacting on wafer. One of the major reasons for the discrepancy is the formation of solidification layer. The droplets and substrates used in [17] were the same material, and the interface temperature for the early portion of the transient is the average of T_s and T_d, without considering the latent heat of fusion. For most of the experiments conducted in [17], this average temperature was higher than T_m, and solidification therefore might start at later stage of spreading process. However, this was not the case in [3], where solidification played a major role throughout the impact process, and Hoffman's law therefore was not quantitatively applicable.

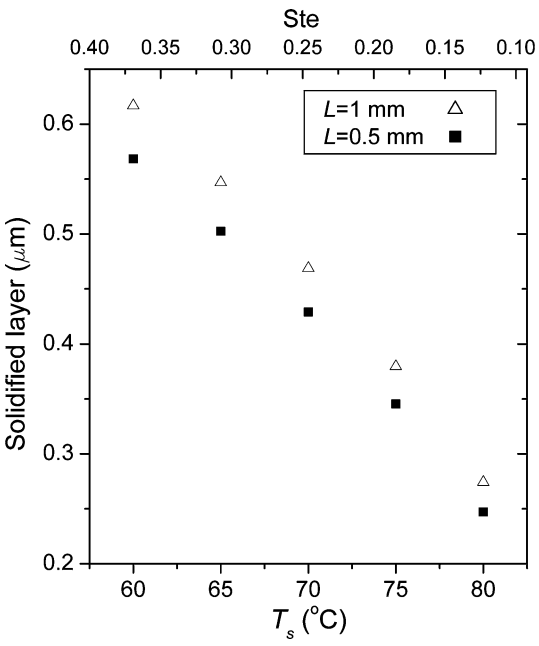

Fig. 7 Solidification fronts (T_m = 90 °C) at the instant of maximum spread of droplets with T_j = 140 °C impacting on the uncoated substrate (Case I)

Figure 7 shows that more liquid was solidified during spreading at $L = 1$ mm than $L = 0.5$ mm, due to a lower T_d at $L = 1$ mm. This implies that contact lines could be arrested at different stages during the process of impact. However, this information does not completely explain the different tendencies of θ_s varying with T_s for $L = 0.5$ and 1 mm (Fig. 5b), which requires understanding of the droplet deformation history during impact. When a droplet spreads to its maximum extent, it does not necessarily come to rest, but may recoil as the edges are pulled back by surface tension forces [3, 21]. When the droplet recoils with its contact line arrested, small solidification contact angle is formed.

Look back at Fig. 4 and try to explain by considering the deformation history of droplets. The photographs shown in Fig. 4b and c indicate that both L and T_s had significant effects on the final shape of dots formed. The edges of dots formed at low T_s (high Ste) with $L = 0.5$ mm indicates that the droplets experienced strong recoiling with the contact lines arrested at the maximum spread (see Fig. 4b), thereby forming small θ_s. The contact lines of droplets impacting at low T_s with $L = 1$ mm seem to have been arrested during the spreading without much subsequent motion of droplet (see Fig. 4c), thereby forming large θ_s. At high T_s (low Ste), the contact lines were arrested at later stage of impact, and the final shapes formed at $L = 0.5$ and 1 mm look similar.

Due to a higher T_d and U at $L = 0.5$ mm, inertia dominated the spreading process, and droplets could spread out to almost the same extent regardless of the value of Stefan number. Contact line was arrested at the instant of maximum spread or during recoil, depending on substrate temperature. For higher T_s, the contact line was arrested earlier. In this case, the contact angle was not frozen at the point of maximum spread, but may decrease due to the recoiling process with contact line arrested. To the contrast, due to the lower T_d and U at $L = 1$ mm, solidification/viscous damping dominated in the spreading process. Consequently, droplet motion stopped rapidly at low T_s due to early arrest of contact line, and the early arrest of contact line during spreading process therefore produced large θ_s. This is similar to the conclusion made in [19] which states that early contact line arrest by freezing can induce dynamic behavior similar to the effect of a large equilibrium contact angle. As T_s increased, the contact line arrest was delayed, and droplets tended to spread to large extent and

recoil, thereby producing smaller θ_s. For $T_s = 80$ °C (Ste = 0.12), the effect of solidification/viscous damping caused by different T_d at $L = 0.5$ mm and 1 mm became less significant, and the droplets impacted at the two distances resulted in almost the same θ_s.

Contact angle (θ_s) versus type of substrate—Cases II and III

In solid-ink printers, non-stick coatings and lubricants are applied to the surface of drum to ensure easy detachment of ink dots. This could also affect the formation of θ_s through affecting impact dynamics and heat transfer during the process of impact. To examine the effect of substrate surface, this section presents experimental results of two other types of substrate surfaces: viton-coated and oil-coated aluminum surfaces.

With the same method as mentioned in the previous section, the equilibrium contact angles of ColorStix 8200 on the two types of surfaces were measured to be 12° on the viton-coated surface and 28° on the oil-coated surface. Since the thermal conductivity of aluminum is much higher than that of viton and silicon coil (see Table 2), we compare the thermal resistance of viton and silicon oil layers with that of the ink droplet.

$$\frac{R_c}{R_d} = \frac{lk_d}{Dk_c} \tag{12}$$

where R_d is the thermal resistance of droplet, and R_c, k_c, and l are the thermal resistance, conductivity and thickness of the coating layer (viton or silicon oil). This thermal resistance ratio was around 0.05 for both types of surfaces, showing that the viton and oil layers did not cause significant effect on heat transfer during droplet impact.

Figure 8 shows measurements of θ_s of ink dots formed on the viton-coated surface in comparison to those on the uncoated aluminum surface: Fig. 8a is for $L = 0.5$ mm and Fig. 8b for $L = 1$ mm. It shows that the two types of surfaces show similar tendencies of θ_s varying with T_s and L. Generally, the contact angles formed on the uncoated substrate were smaller than those on the viton-coated substrate, showing the effect of wettability. However, exceptions can be found at $T_s = 60$ °C and 65 °C with $L = 1$ mm, where larger contact angles were formed on the uncoated substrate, due to earlier arrest of contact line on the uncoated surface. Although our analysis showed insignificant thermal effect of the viton-coating, droplets impacting at low T_s at $L = 1$ mm could still be sensitive to this thermal effect.

Wettability of substrate surface (θ_e) affects the impact dynamics of droplets. For isothermal spreading, it has been widely accepted that dynamic contact angle increases with

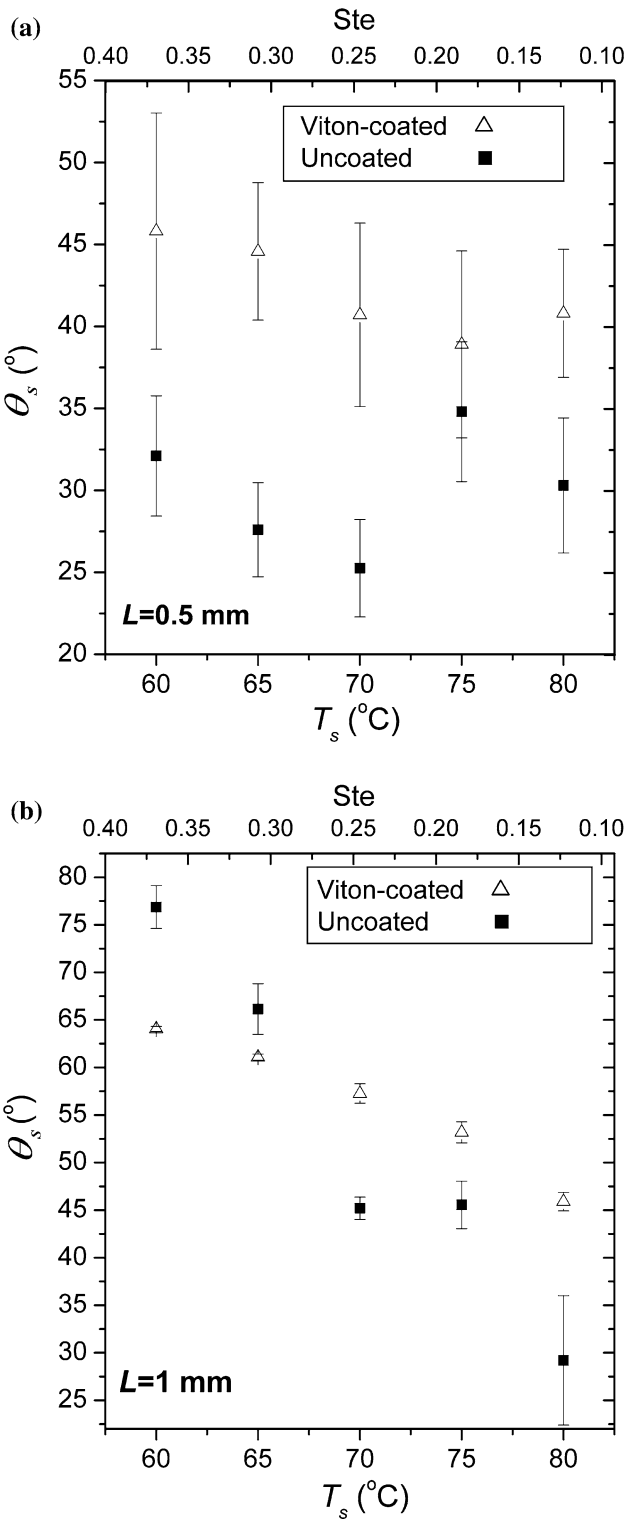

Fig. 8 Solidification contact angles formed on the viton-coated substrate (Case II) in comparison to those on the uncoated substrate (Case I): (**a**) $L = 0.5$ mm; (**b**) $L = 1$ mm

θ_e [18]. Fukai et al. [14] found that the maximum spread of droplet decreases as the dynamic contact angle increases. The droplet spreading model in [23] shows a significant

effect of dynamic contact angle on the droplet spreading, provided We < 500 and Re ~ 10. Amada et al. [24] reported a similar finding by evaluating the correlation model of maximum spread diameter proposed in [9]. With the involvement of solidification in the present study, droplet impacting on the viton-coated substrate resulted in less deformation than those on the uncoated substrate. Therefore, for most tests (except T_s = 60, 65 °C at L = 1 mm), larger contact angles were formed on the viton-coated surface than those on the uncoated surface. Figure 8b indicates that wetting effect became significant at high substrate temperature. This is similar to the numerical and experimental results of [13, 25], which reported increasing importance of wetting with decreasing Ste.

In addition to wettability, viscoelastic effect could be another factor in affecting the formation of solidification contact angle. The shear modulus of aluminum ($G \sim 20$ GPa) is four orders of magnitude higher than that of viton ($G \sim 2$ MPa). However, for droplet impaction driven by inertia such as the present work, the viscous dissipation that occurs inside the droplet dominates over the viscoelastic dissipation that occurs inside the ''soft'' substrate [26]. This can also find support by comparing the elastic displacement H with thickness of solidified layer. The elastic displacement of the viton normal to the substrate surface can be estimated by [26]

$$H \sim \frac{\sigma \sin\theta_e}{G} \tag{13}$$

which gives ~2 nm. This is much smaller than the thickness of solidified layer (see Fig. 7), which was formed in a very short time scale (~15 μs) determined by Eq. 6. Therefore, the viscoelastic effect of the viton-coated substrate was negligible.

Figure 9a shows photographs of droplets impacted on the oil-coated substrate located at L = 0.5 mm from the droplet generator, and the data of θ_s were plotted in Fig. 9b. Despite the largest θ_e on the oil-coated surface, comparison between Fig. 9b (Case III) with Fig. 8a (Case I versus Case II) does not show the effect of wettability on θ_s, which, however, is clearly shown in Fig. 8a. This is because the existence of a liquid layer on a solid surface affects not only the wettability, but also the fluid dynamics near the contact line of impacting droplets. Slip boundary occurs due to the existence of this oils layer. In the present work, a portion of kinetic energy of the droplet was consumed on the droplet edge to push away some silicon oil during the process of spreading. The vestige of this effect is clearly visible on the dot edges in Fig. 9a, but disappears for T_s = 80°C.

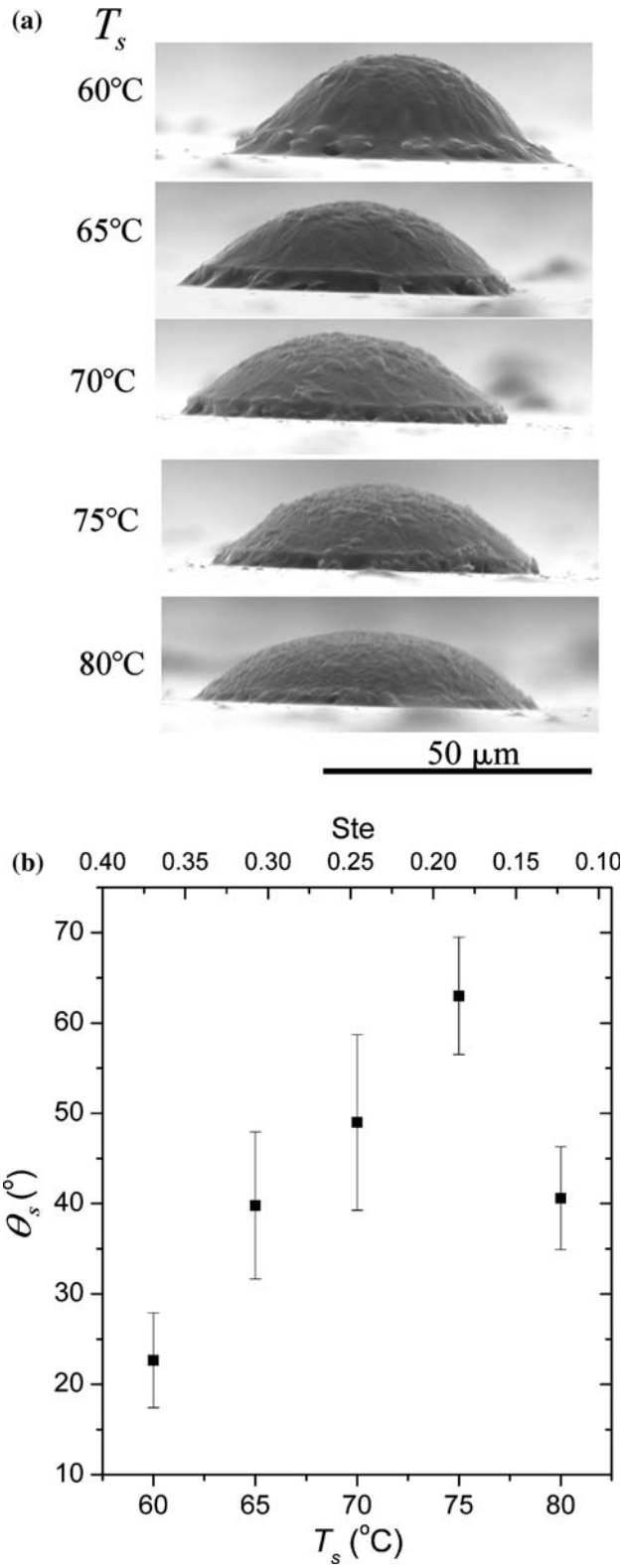

Fig. 9 (**a**) Side view SEM images of ink dots formed on the silicon oil coated substrate with T_j = 140 °C and L = 0.5 mm (Case III); (**b**) solidification contact angles formed on the oil-coated substrate—measurement of Fig. 9a

Figure 9b shows θ_s increased with T_s, but decreased when T_s was high. For the temperature range employed in the present work, there is no need to consider the evaporation effect of the silicon oil. In the present case, the substrate temperature affected not only the thermal history of droplets, but also the viscosity of the oil layer. For low substrate temperatures, the spreading process was mainly determined by solidification and temperature change inside the droplet, because the quickly solidified and highly viscous liquid adjacent to substrate surface could be too stiff to be affected by the silicon oil. As T_s increased, the droplets tended to spread to larger extents, and the resistance from the silicon oil tended to prevent the contact line from further spreading, thereby causing θ_s to increase. At T_s = 80°C, due to the slow decrease of droplet temperature during impact and low viscosity of the oil layer, the droplet had time to restore its free surface adjacent to its contact line, resulting in the decease of contact angle at this substrate temperature.

Contact angle (θ_s) versus jetting temperature (T_j)—Case IV

Effect of superheat parameter β (changing T_d) can be investigated by increasing the jetting temperature (T_j). We increased T_j from 140 to 145 °C without causing measurable change of droplet size and velocity, and β therefore was increased by 10%.

Figure 10 exhibits θ_s formed by droplets with T_j = 145°C impacted on the uncoated substrate at L = 1 mm (Case IV) in comparison to Case I (T_j = 140°C), which has been presented in Fig. 5b. The contact angles formed with T_j = 145°C (higher β) were generally smaller than those formed with T_j = 140 °C (lower β). This difference was because of the larger spreading favored by higher droplet temperature (T_d). The difference diminished at high T_s (low Ste), indicating that the effect of β decreased with Ste. It can also be concluded that θ_s showed higher sensitivity to Ste at low β. This is simply because the increase of β (increase of droplet temperature) reduced the effects of solidification and viscous damping, which in turn reduced the effect of Ste (T_s) on the final shape of dots formed.

Deviation from spherical cap shape

The order-of-magnitude analysis has shown that, in the present work, the time required for spreading was much shorter than that required for the entire droplet to solidify. This has served as a basis for neglecting the effect of solidification on droplet impaction in a few early studies. In other words, the droplet spreads first and subsequently cools and solidifies provided $t_{spr} \ll t_{solid}$. Without considering the effect of solidification, the impacted droplets should finally reach their equilibrium shapes (spherical caps provided Bo $\ll$ 1), and its θ_s can be calculated by using the following geometric relations (A similar model was proposed in [6])

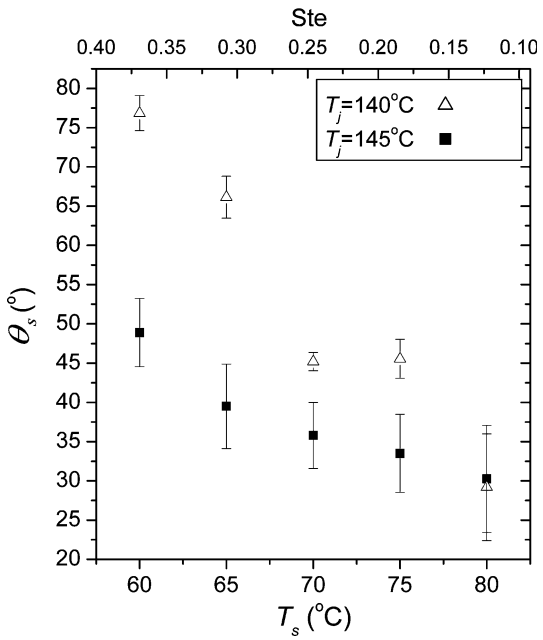

Fig. 10 Solidification contact angles formed by droplets impacted on the uncoated substrate at L = 1 mm with T_j = 145 °C (Case IV) and T_j = 140 °C (Case I)

$$\text{If } \frac{D^3}{h^3} \le 4,\ \theta_c = \pi - \sin^{-1}\left(\frac{\sqrt{12D^3h^3 - 12h^6}}{2h^3 + D^3}\right)$$
$$\text{If } \frac{D^3}{h^3} \ge 4,\ \theta_c = \sin^{-1}\left(\frac{\sqrt{12D^3h^3 - 12h^6}}{2h^3 + D^3}\right) \quad (14)$$

where h is the height of sessile droplet, and θ_c is the apparent contact angle obtained via this method. The base diameter of sessile drop has been replaced by pre-impact diameter of droplet based on conservation of mass. The first relation is for blunt angles, while the second for sharp angles.

The height of ink dots formed on the uncoated and viton-coated substrates (T_j = 140 °C, Cases I and II) was measured and was put into Eq. 14 to calculate θ_c. The difference between the calculated and measured angles, $\theta_c - \theta_s$, was plotted in Fig. 11. It shows that the final shape deviates from spherical cap to various degrees depending on impact conditions. For instance, under the condition of L = 0.5 mm and T_s = 60°C on the uncoated surface θ_s was 35° smaller than θ_c, for L = 1 mm on the viton-coated surface θ_s was very close to θ_c. Several phenomena can be observed from Fig. 11: (1) θ_s is generally smaller than θ_c,

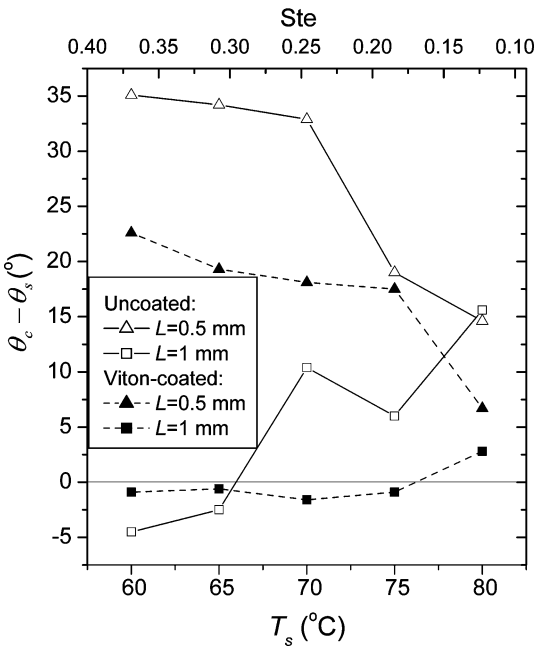

Fig. 11 The angle θ_s was directly measured, while θ_c was calculated by using Eq. 14

due to the process of recoiling with contact line arrested. (2) Due to a high wettability of aluminum surface, contact line was arrested when droplets spread out to larger extent, and dots formed on the uncoated substrate differed from spherical caps to a larger extent than those formed on the viton-coated substrate. (3) Due to higher U and T_d at $L = 0.5$ mm, droplets experienced more deformation during the process of impact, thereby causing larger differences $\theta_s - \theta_c$ than those impacting at $L = 1$ mm. (4) As T_s increased, $\theta_c - \theta_s$ decreased for $L = 0.5$ mm, but increased for $L = 1$ mm. Arrest of contact line mainly opposed spreading for $L = 1$ mm but recoiling for $L = 0.5$ mm. Increasing T_s reduced these resistances by delaying contact line arrest, causing flattening effect for $L = 1$ mm and restoring effect for $L = 0.5$ mm. (5) For high T_s, the final shape of droplet was less dependent on deformation history. Hence, as T_s increased, $\theta_c - \theta_s$ for $L = 1$ and 0.5 mm tends to converge to one point.

As clearly indicated by Fig. 11, although droplets solidified long after they reached maximum spread, the shape of spherical cap was not restored. The final contact angle θ_s showed strong dependence on the impact history of droplets.

Conclusions

This work presents an experimental study on molten droplets impacting cold surfaces. Focus was put on the solidification contact angle (θ_s) formed by micron sized droplets of wax ink impacted on solid surfaces under varied impact conditions. Although the order of magnitude analysis showed that the spread time of droplets was much shorter than the bulk solidification time, θ_s was found not to be single-valued for given droplet and substrate materials and substrate temperature but strongly dependent on the deformation history of the droplet during the process of impact. A heat transfer analysis indicates that solidification affects the arrest of contact line, thereby changing the evolution of free surface near the contact line.

It was found that θ_s decreased with increasing substrate temperature (decreasing Stefan number) and decreased with increasing jetting temperature (increasing superheat parameter). Smaller contact angles were formed when substrate was located closer to the droplet generator. The effects of droplet travel distance and jetting temperature lessened with increasing substrate temperature. For lower jetting temperature, the sensitivity of θ_s to the substrate temperature decreased.

By using two types of substrate surfaces (uncoated aluminum and viton-coated surfaces) with different wettabilities, smaller contact angles were found to be favored by higher wettability, and the wetting effect increased with increasing substrate temperature. Applying a thin silicon oil layer to the substrate surface was found to increase equilibrium contact angle, but the solidification contact angle was found to be mainly influenced by the resistance of oil layer to the motion of droplet contact line.

Geometric relations of spherical cap were used to estimate the final contact angle (θ_c), and the difference between θ_c and the directly measured θ_s indicated that the final shape deviated from the shape of spherical caps to various degrees depending on impact conditions.

Acknowledgements The authors greatly thank Dr. Stephan Drappel from Xerox Research Centre of Canada for his help and discussion. The authors are indebted to Chris Wagner and Bradley Gerner from Xerox Corporation for their assistance in setting up the jetting fixture and to David Gervasi from Xerox Corporation for the viton coating. This work is supported by Xerox Foundation and Natural Sciences and Engineering Research Council of Canada (NSERC).

References

1. Pasandideh-Fard M, Pershin V, Chandra S, Mostaghimi J (2002) J Therm Spray Technol 11(2):206
2. Mostaghimi J, Pasandideh-Fard M, Chandra S (2002) Plasma Chem Plasma Process 22(1):59
3. Attinger D, Zhao Z, Poulikakos D (2000) ASME J Heat Transfer 122:544
4. Hayes DJ, Wallace DB (1998) Chip Scale Rev 2(4):75
5. Waldvogel JM, Diversiev G, Poulikakos D, Megaridis CM, Attinger D, Xiong B, Wallace DB (1998) ASME J Heat Transfer 120:539

6. Gao F, Sonin AA (1994) Proc R Soc Lond A 44:533
7. Snyder T, Korol S (1999) In: IS&T's Recent progress in Ink Jet Technologies II. In Hanson E (ed) Springfield, VA, pp 175–181
8. Chandra S, Avedisian CT (1991) Proc R Soc Lond A 432:13
9. Bennett T, Poulikakos D (1993) J Mater Sci 28:963; Doi: 10.1007/BF00400880
10. Zhao Z, Poulikakos D, Fukai J (1996) Int J Heat Mass Transfer 39(13):2791
11. Waldvogel JM, Poulikakos D (1997) Int J Heat Mass Transfer 40(2):295
12. Aziz SD, Chandra S (2000) J Heat Mass Transfer 43:2841
13. Haferl S, Poulikakos D (2002) J Appl Phys 92(3):1675
14. Fukai J, Shiiba Y, Yamamoto T, Miyatake O (1995) Phys Fluids 7(2):236
15. Sikalo S, Tropea C, Ganic EN (2002) Exp Therm Fluid Sci 29:795
16. Sikalo S, Wilhelm H–D, Roisman IV, Jakirlic S, Tropea C (2005) Phys Fluids 17:062103
17. Schiaffino S, Sonin AA (1997) Phys Fluids 9(8):2217
18. Hoffman RL (1975) J Colloid Interface Sci 50:228
19. Schiaffino S, Sonin AA (1997) Phys Fluids 9(11):3172
20. Bhola R, Chandra S (1999) J Mater Sci 34:4883
21. Kim H-Y, Chun J-H (2001) Phys Fluids 13(3):643
22. Carslaw HS, Jaeger JC (1959) In: Conduction of heat in solids. 2nd edn, Clarendon Press, Oxford, pp 288–289
23. Gong S-C (2005) Jpn J Appl Phys 44(5A):3323
24. Amada A, Haruyama M, Ohyagi T, Tomoyasu K (2001) Surf Coat Tech 138:211
25. Haferl S, Poulikakos D (2003) Int J Heat Mass Transfer 46:535
26. Carre A, Gastel J-C, Shanahan MER (1996) Nature 379:432